

Distinct changes of genomic biases in nucleotide substitution at the time of mammalian radiation

Peter F. Arndt^{1,2}, Dmitri A. Petrov³, and Terence Hwa¹

¹*Physics Department, University of California at San Diego, La Jolla, CA 92093*

²*Institute for Theoretical Physics, Cologne University, 50937 Cologne, Germany*

³*Department of Biological Sciences, Stanford University, Stanford, CA 94305*

Abstract

Differences in the regional substitution patterns in the human genome created patterns of large-scale variation of base composition known as genomic isochores. Utilizing the vast amount of repetitive sequence in the human genome, we developed a maximum likelihood approach providing estimates of substitution frequencies of the four transversions, two transitions, and the methyl-assisted transition of cytosine in CpG. Comparing substitutional patterns in repetitive elements of various ages, we are able to reconstruct the history of the base-substitutional process in the different isochores for the past 250 Myr. At around the time of the mammalian radiation (~90 Myr ago), we find an abrupt 4- to 8-fold increase of the cytosine transition rate in CpG pairs compared to that of the reptilian ancestor. Further analysis of substitutional patterns in regions with different GC-content reveals that concurrently the substitutional pattern changed from an isochore-preserving to an isochore-degrading one. We conclude that isochores have been established before the radiation of the eutherian mammals and have been subject to the process of homogenization since then.

Different regions of the human genome show large variation in GC-content from 30% to 60% at scales exceeding hundreds of kilobases (1-3). The origin, timing and implications of this so called “human isochore structure” is still controversial, primarily due to a number of technical issues that have made it difficult to reconstruct the history of nucleotide substitutions. The difficulties in assessing substitutional biases in vertebrate genomes that acted on coding and non-coding sequences far in the past come from two sources. One is that many substitutional processes in non-coding regions are fairly fast, leading to multiple changes at the same site (so-called “multiple hits”), which quickly obscure the true pattern of substitution. The other is the strong *neighbor-dependence* of some substitution processes, especially the methylation-assisted transition of cytosine found in 5'-CG-3' (CpG) pairs, leading to a sharply elevated (by as much as 10-fold) rate of substitution from CpG to TpG and CpA (4). Such neighbor-dependence exacerbates the problem of multiple hits and severely complicates any inference of substitutions beyond the very immediate past (i.e., more than 10-15 Myr ago).

To address these issues we developed a maximum likelihood (ML) method that simultaneously estimates the substitution rates corrected for multiple hits, for the four transversions, two transitions, and the CpG-based transition process. This method is based on a recently developed treatment of neighbor-dependent substitutions (5), which is an extension of Kimura’s approach along with its generalizations (6, 7) to include the CpG-based transition process. Importantly, it is capable of recovering the true patterns of substitution going far back in time, given the knowledge of the ancestral sequence and a sufficient amount of data.

In the case of the human genome, sufficient amount of data is indeed available in the form of exceptionally prolific interspersed repetitive elements (REs), which have been inserted into the human genome in bursts at various stages during evolution (8-12). Every burst generated numerous copies of an ancestral “Master sequence”, which we can reconstruct easily from the available data. The Master sequences was not the same for every burst; this way various sub-

families of RE have been generated at different times in evolution. Most of the REs reside in the intergenic regions and are believed to be functionally neutral.

The oldest families of REs that can be identified in the human genome have been inserted over 200 Myr ago (MYA). Naturally, older elements accumulated more base substitutions than younger ones. Therefore, a careful comparison of the frequencies of substitutions observed in REs of different ages can tell us the history of the substitutional processes extending far into the past. This analysis applied to all REs found in the human genome provides us with the information about the genome-wide averaged background substitutional processes at different times. Using the same analysis and applying it to REs found in specific regions we could reconstruct the region-specific substitutional processes, as well. We were able to reveal different substitution patterns in regions with different background GC-content. These patterns changed in time and therefore provide us additional information on the origin and timing of the human isochore structure.

Materials and Methods

Data Collection. This work is based on the analysis of ~2,800 Mbp of autosomal sequence data from the human genome, available at GenBank (Build 28; February 11, 2002). The “RepeatMasker” (<http://repeatmasker.genome.washington.edu>) was used to identify copies of various REs and to classify them into families and sub-families as they appear in the RepBase database (13). With this procedure, 46% of the genome was identified to be either a part of an RE or a sequence of particularly low complexity. The subsequent analysis was focused on elements from the 42 subfamilies of retrotransposons (see Table 1), including 7 sub-families of Alu's (14), 32 subfamilies of the LINE element L1 (15), as well as older elements such as L2, L3 (13), and MIR (16). We excluded partial alignments shorter than 250 bp for the Alu's, or shorter

than 100 bp for the others. The number of remaining alignments and their average lengths are listed in Table 1 and sums to a total of 410Mbp of sequence data (> 10% of the human genome) that was used in the analysis. We further verified that the identification of the oldest REs (MIR, L2, L3) is well within the capability of RepeatMasker. We synthetically aged the ancestor sequences of these RE families (see *Supporting Information*) to a significantly higher degree of divergence (including indels) than what was found in the data and verified that we could identify these using the RepeatMasker. To avoid potential biases on the set of identified repeats by the regional GC-content, the “-gc 43” option of the RepeatMasker was turned on, and the scoring system appropriate for the genome-wide average GC-content of 43% was chosen. Note, however, that whether the “-gc 43” option was on or not did not significantly affects the results. For the output of local gapped alignments of each identified copy with its ancestor sequence needed for our further analysis we turned the “-a” option on, as well.

Due to the large number of copies of REs in each subfamily, it was also possible to subdivide these copies into seven groups according to the GC-content of regions flanking each identified copy. In counting the GC-content of the flanking regions, we masked away the sequences of other REs appearing in the regions. The modulation of the length of the flanking regions from 2kb to 10kb did not affect the results. We verified that the shift in GC-content in the last 100 Myr due to the current substitution pattern is less than 5% (results not shown). Thus, the regional GC-content as measured in today’s genome reflects approximately those at about 100 MYA. For the genome-wide analysis of substitution frequencies, we further accounted for the different densities of REs in the different isochores (17) and randomly discarded identified copies of REs such that the total amount of repetitive sequence was proportional to the total amount of genomic sequence of a given GC-content.

Data Analysis. In the analysis, the “star” phylogeny was assumed for each subfamily of REs. This assumption is based on the known biology of retrotransposons, and supported by previous

phylogenetic analysis of the transposons (10, 11, 14). The assumption is invalidated if a significant fraction of the REs is generated by duplication. However, the latter is estimated to affect under 10% of the REs (J. Jurka, personal communication), making the star phylogeny a reasonable starting point. Given the degree of sequence divergence of the copies of REs (Table 1) we assume that each copy evolves as a unique sequence. Further, the extremely low divergence of the youngest REs (13) in the human genome suggests that retrotranscription errors can be safely ignored. The ancestor sequence for each subfamily is taken from the RepBase (13) and verified by a ML-based reconstruction method.

Estimation of substitution frequencies. We used a maximum likelihood (ML) approach to estimate the substitution frequencies for each sub-family of REs. The observed data is given by the pair-wise gapped alignments of each identified copy of a RE in the genome (β_1, \dots, β_M) with its ancestral sequence ($\alpha_1, \dots, \alpha_M$) from the RepBase (13). Here Greek letters represent the nucleotides: A, C, G and T, and M is the length of the alignment. From the alignments of a particular subfamily of RE, we count the number of observed substitutions $\alpha_i \rightarrow \beta_i$, recording also the neighboring bases in the ancestor, α_{i-1} to the left and α_{i+1} to the right. We disregard a site i if any of the α_{i-1} , α_i , α_{i+1} , β_i is an insertion or deletion in the alignment. We denote these counts by $N(\beta|\alpha_L, \alpha, \alpha_R)$ and the set of all counts for a subfamily by $\{N\}$.

To implement the maximum likelihood approach, we need to specify a substitution model describing the observed data. We chose a general model comprising all possible single nucleotide transversions (8) and transitions (4) as well as the CpG-based transition, CpG→CpA/TpG. Each process and its complementary process are assumed to occur with the same substitution frequency per site. Hence the substitution model is parameterized by a set of seven frequencies, collectively denoted as $\{\omega\}$. The likelihood of observing the data $\{N\}$ under a given model with parameters $\{\omega\}$ can be approximated by

$$L(\{N\} | \{\omega\}) = \prod_{\beta, \alpha_L, \alpha, \alpha_R} P(*\beta* | \alpha_L, \alpha, \alpha_R; \{\omega\})^{N(\beta|\alpha_L, \alpha, \alpha_R)}$$

where $P(*\beta*|\alpha_L, \alpha, \alpha_R; \{\omega\})$ is the probability that a sequences of three bases set up initially with the configuration $\alpha_L, \alpha, \alpha_R$ evolves under the model $\{\omega\}$ to a state with the base α substituted by β . To include effects due to multiple- and back-substitutions of the same base, this probability is calculated by iterating a set of 64 differential equations that encodes the time evolution of the three nucleotides taking the set $\{\omega\}$ as a parameters (5). The likelihood $L(\{N\}|\{\omega\})$ can then be maximized using standard algorithms (18), adjusting $\{\omega\}$ to find the set of substitution frequencies which most likely describes the observed data. The typical error of the ML estimate can easily be computed by bootstrap (18). Due to the large amounts of sequence data for every family of REs, the errors are smaller than the symbol size in the figures presented and therefore were omitted from these graphs.

The heart of our method is the *neighbor-dependent* substitution model (5), which has recently been developed extending of Kimura's approach and its generalizations (6, 7) to include the CpG-based transition process. It was assumed that the REs were selectively neutral, so that the two DNA strands can be treated in the same way. The model comprised the 4 transversions, 2 single-nucleotide and the CpG-based transitions, as well as all the secondary processes involving multiple- and back- substitutions. A special case of this model in which all the transition rates were equal and all the transversion rates were equal was solved analytically as described in Ref. (5). For the more general case at hand involving all 7 substitution frequencies, the principle of the likelihood calculation was the same as in Ref. (5), but the calculation became more tedious and was performed with the help of a computer. The corresponding program is available upon request. Undoubtedly, the inclusion of the neighbor-dependent substitution process made the analysis more complicated. However, the results obtained were more sensitive and reliable at longer evolutionary time scales, especially when compared to the alternative method of "direct counting" of CpG \rightarrow CpA/TpG events. The performance of this approach is further analysed and presented as *Supporting Information*.

Reconstruction of the ancestral sequence. In our analysis, we assumed that the RE sequence appearing in the RepBase was the correct ancestral sequence (13). We tested this assumption by reconstructing the ancestral sequence from all copies found in the human genome, using the ML approach with the above substitution model. In contrast to the above estimation of substitution frequencies, here we want to find the most likely ancestral sequence $(\alpha_1, \dots, \alpha_M)$, given the observed copies and our substitution model. The likelihood to be maximized is again $L(\{N\}|\{\omega\})$ but now one has to adjust the ancestral sequence α_i (which changes the numbers $\{N\}$) while keeping the substitution frequencies $\{\omega\}$ fixed. Initially the frequencies $\{\omega\}$ are unknown. We use the naïve consensus sequence and the ML analysis described above to get an estimate for these frequencies. Subsequently, we construct the ML-ancestor by varying the ancestor sequence and maximizing $L(\{N\}|\{\omega\})$ using the $\{\omega\}$ just determined. We then use the new ancestor sequence to get a better estimate of the frequencies. After three iterations, this procedure converges to a unique ML-ancestor sequence and estimated substitution frequencies. We tested this method using synthetically evolved sequences (see below) and were able to reconstruct the known ancestor sequence exactly, even if all CpG disappeared from the naïve consensus sequence due to a high CpG-based transition frequency. Comparing the ML-ancestor and the ancestor in the RepBase, we observe differences for less than 2% of the sites.

Results

To investigate the *history* of substitution processes during the course of human evolution, we extracted from the human genome numerous copies of the commonly encountered families of retrotransposons, the SINEs (Alu, MIR) and LINEs (L1, L2, L3), see Table 1 for a complete listing. For each of the 42 subfamilies of REs obtained, we computed the average number of substitution events per site (corrected for back and multiple substitutions) for each of the 3 transitions (the 2 single-nucleotide transitions and the CpG-based transition $\text{CpG} \rightarrow \text{CpA/TpG}$)

and 4 transversion processes using our maximum likelihood method; the results are referred to as transition and transversion “frequencies” respectively. In Fig. 1, we plot the 3 transition frequencies against the average of the four (very similar) transversion frequencies for each subfamily. From Fig. 1, we observe first that the two single-nucleotide transition frequencies (the blue and red symbols) show remarkably *linear* dependence on the average transversion frequencies. This suggests that the genome-wide averaged single-nucleotide substitution pattern (as defined in *Methods*) has not changed since the time the oldest elements (L3, L2, MIR) entered the genome. Fitting these two transition frequencies to straight lines, and identifying the slopes as the transition rates (relative to the average transversion rate), we find that the A:T → G:C transition (red symbols) occurs 2.74 ± 0.04 times more frequently, and the G:C → A:T transition 5.5 ± 0.1 times more frequently than an average transversion event. Given the linearity of the data, it is tempting to assume that the single-nucleotide substitution *rates* are time-independent throughout the time span studied, and identify the horizontal axis of Fig. 1 as the “time” axis. Calibrating the time scale using estimates of the absolute insertion time of the different Alu sub-families (8), we find each unit of $t=0.01$ in the average transversion frequency to correspond to approximately 35 Myr, with the entire dataset spanning nearly 250 Myr.

The corrected frequencies obtained for the CpG-based transition process (green symbols in Fig. 1) present a big surprise: There are clearly two regimes characterized by very different slopes. This finding is supported by REs across different families of SINEs and LINEs, including the Alu’s, which insert preferentially in GC-rich regions as well as the L1’s, which prefer AT-rich regions. We verified that this finding is not an artifact of the ML analysis: extensive simulation shows that our method is capable of detecting transition frequency for the CpG-based process up to 4-5 times that of the highest frequencies found in our data (see *Supporting Information*). To quantify the extent to which the transition rates changed in the past, we divided the data into the two sets of young and old REs with respect to a threshold value t_0 . Subsequently t_0 was adjusted such that the sum of the squared residuals of linear regressions to the data in both

sets is minimal. For the data on the CpG-transition process (as shown by the green symbols in Fig. 1), this minimum was found for $t_0=0.025$, with a slope of 39.5 ± 2.6 for the young elements and 8.4 ± 2.5 for the old elements (relative to the average transversion rate). The data are almost certainly ($P = 10^{-13}$) not described by a single straight line. We can identify the slope with the relative rate (see *Supporting Information*) and conclude that a 4- to 8-fold increase in the CpG-based transition rate occurred at $t_0=0.025$. On the other hand, we could not detect any significant change in the rates between the young and old elements for the two single-nucleotide transition processes (the blue and red symbols in Fig. 1). The single straight lines fit the rates of both transitions relative to the average transversion rate remarkably well ($R = 0.99$), suggesting that a split of the data into sets of young and old elements is not justified.

Intriguingly, $t_0=0.025$ (~ 90 MYA) corresponds roughly to the time of the mammalian radiation (19-23). Corroborating this inference is an independent observation in Fig. 1 that the CpG-based transition frequencies of nearly all the L1Pxx elements (solid square symbols, corresponding to the L1's found in all primates) fall on the steep segment, while the CpG-based frequencies of all the L1Mxx elements (solid diamond symbols, corresponding to L1's found in all eutherian mammals) (15) fall on the flatter segment. One possible mechanism for the abrupt increase of the CpG-based transition rate (but not the neighbor-independent $C \rightarrow T$ transition rate) is a hypothetical elevation of methylation activity in germ-line cells at the time of mammalian radiation.

To gain some insight into the strong regional GC-content variations of the human genome, we repeated the above analysis separately for REs found in regions with different base composition. Specifically, we partitioned the REs according to the base composition of the region flanking individual copies into 7 equally-sized bins of GC-content ranging from 30% to 60%. A plot similar to Fig. 1 was generated for each of the GC-content bins and analyzed separately. As expected, we find the abrupt upward shift in the rate of CpG-based transition for

every bin of GC-content, occurring at approximately 90 MYA (data not shown). More surprisingly, the rates of single-nucleotide transitions also showed time dependence. As shown in Fig. 2, both transition frequencies are nearly independent of GC-content for transversion frequencies <0.02 , i.e., in the recent past, while clear dependence on GC-content can be seen for the two transitions at much earlier times, e.g., for transversion frequencies >0.03 . Moreover, the dependences of GC-content in the distant past are opposite for the two transitions: The rates of GC-enriching transitions were higher in the regions of higher GC-content (Fig. 2a) while the opposite was the case for the AT-enriching transitions (Fig. 2b). It thus appears that the GC-dependence of the substitution pattern also underwent a change; intriguingly it coincides in time (~ 90 MYA) with the upward shift of the CpG-based transition rate and the mammalian radiation. Note that this change is not a trivial consequence of the shift in the genome-wide CpG-based transition rate shown in Fig. 1 since the different substitution processes are treated separately in our ML analysis.

We quantified all of the substitution rates in the recent and distant past by fitting the data such as those in Fig. 2 to straight lines, separately for those with transversion frequencies below 0.02 and above 0.03. This was done for all 7 bins of GC-content, allowing us to analyze the dependences systematically. In the distant past, i.e., prior to ~ 90 MYA (Fig. 3), the GC dependence of substitution rates appears to have been preserving or generating both the GC-rich and GC-poor isochore structures: AT-enriching substitutions (blue symbols) were predominant in the GC-poor isochores, and the reverse was true for the GC-rich isochores (Fig. 3a). We examined the degree of preservation quantitatively by computing (5) the stationary GC-content corresponding to each of the substitution patterns in each of the 7 bins of GC-content found in Fig. 3a. The results are shown in Fig. 3b. We come to the conclusion that back at ~ 90 MYA, steady state had been reached and the GC-content of each region was indeed preserved by the regional substitution patterns. Note also that the very good agreement between the observed GC-content of the flanking regions and the predicted stationary GC-content from the patterns of

substitutions within the REs validates two important aspects of our approach. First, it shows that we can faithfully estimate patterns of substitutions within REs going back 90 – 250 Myr. It also shows that the patterns of substitution within REs are fair estimates of substitutional processes in their flanking regions.

The situation has been very different in the recent past, i.e. since ~90 MYA, where a changed substitution pattern can be observed (Fig. 4). The difference between the two substitution patterns of the distant and recent past (compare Figs 3a and 4a) is highly significant ($p < 10^{-6}$). For the recent past, there is only weak dependence of the substitution frequencies on the GC-content, which has been also observed recently by Yi et al (24). However, despite of these dependencies and especially since the frequencies of AT-enriching transversions and transitions (blue symbols in Fig. 4a) always exceed those of the GC-enriching substitutions (red symbols), it is clearly not possible to preserve the regional GC-content with such a substitution pattern. The plot of stationary versus regional GC-content (Fig. 4b) is computed using the rates given in Fig. 4a. The most striking feature of this plot is the inference that the high-GC isochores are currently disappearing from the human genome. Assuming the persistence of the present substitution pattern, the GC-content will be homogenized in the range of 35 - 40% in about 400 Myr (calculation not shown). The ongoing loss of high GC isochores is also implicit in the results derived from the analysis of transposable elements by Lander et al (25). Similar conclusions have been recently noted by Duret et al (26) who estimated the rates of synonymous substitutions in orthologous genes in closely related species within primates, cetartiodactyls and rodents. The parallel shift toward lower GC-contents in several orders of eutherian mammals suggests that the shift occurred in their common ancestor (26). Our analysis agrees with this interpretation and further quantifies it by showing that the shift occurred around the time of mammalian radiation.

Discussion

The ability to directly estimate the rates of all types of substitutions so far back in time allows us to shed light on several contentious issues. The inferred substitution patterns provide strong support for the inference by Galtier and Mouchiroud that the ancestor of eutherian mammals had a very pronounced variation in GC content, more similar to that found in humans than in rodents (27). Our results also suggest that the substitution pattern leading to the eventual establishment of high-GC isochores evolved in the common ancestor of amniotes, resulting in the parallel evolution of the strongly heterogeneous GC-content in mammals, birds and reptiles (28-30).

What are the possible explanations for the sharp reduction in the GC-dependence of *all* transition and transversion rates (Fig. 2 and 4), without any apparent change in the genome-wide rate of transitions and transversions at approximately 90 MYA (Fig. 1)? We believe that the most likely explanation is a combination of the regional mutation hypothesis (31) (or regional substitution hypothesis) and increased chromosomal rearrangement activities in the mammalian lineage. Imagine that some regions in the genome (for instance centromeric and telomeric regions) have consistently higher rates of AT to GC substitutions. Without chromosomal rearrangements, the DNA sequences in these regions will eventually reach steady state and attain a higher GC content consistent with the local substitution rates. Suppose the rate of chromosomal rearrangements increased significantly after steady state was reached, e.g., at around 90 MYA. Then until a new steady state can be reached (a process which would take several hundred Myr), some RE's in GC-rich segments would be subject to low AT \rightarrow GC substitution rates while others would continue to have high AT \rightarrow GC rates, and similarly for RE's in GC-poor segments. This would remove the apparent GC-dependence of the substitution rates since 90 MYA, and explain why all transition and transversion rates changed their GC-dependences synchronously at that time while the genome-averaged substitution rates hardly changed at all. An alternative scenario is the occurrence of an isolated episode of increased chromosomal rearrangements at around 90 MYA. This would also produce the observed shift in the GC-

dependence of the single-nucleotide substitution patterns. However, under this scenario, we would expect the isochore structure existing prior to 90 MYA to re-establish itself rather than becoming completely degraded after several hundred Myr.

Our model suggests that the rate of chromosomal rearrangements in the amniote ancestor was lower than it is in eutherian mammals. We predict that the mammalian lineages with higher rate of molecular evolution will show a more muted isochore pattern with less variation of the GC content across the genome. This prediction is borne out in the case of the mouse lineage, which shows both the muted isochore pattern (32) and elevated rates of molecular evolution (33, 34).

The most intriguing result generated by our analysis is the apparently coincidental increase of the CpG-based transition rate (possibly due to an increase in methylation rate of cytosine) and the decrease in the GC-dependence of the single-nucleotide transitions and transversions (probably due to the increase in chromosomal rearrangement activities). Although we do not have an explanation for this coincidence, we would like to point out a possible causal connection: If the mammalian lineage experienced an invasion of very active transposable elements (such as L1s) at this time, the increase in methylation rate could be an evolved response to control the expansion of transposable elements (35). The increase in the rate of chromosomal rearrangements then can be due to the increase in the number of dispersed homologous sequences generated by the active transposable elements and the consequent increase in the rate of ectopic recombination.

Acknowledgements. This work was supported by the NSF (PA,TH), the Burroughs-Wellcome Fund (TH), the DFG (PA), and Stanford University OTL (DP).

RE	copies	av. length	divergence	tv frequency
L1PA2	3185	512	2.50%	0.0044
L1PA3	5935	505	3.50%	0.0048
L1PA4	7322	454	4.40%	0.0071
AluY	112061	298	8.80%	0.0085
L1PA5	6865	438	5.70%	0.0088
AluSp	42396	299	11.30%	0.0093
AluSc	39381	295	11.60%	0.0102
AluSg	70933	296	12.50%	0.011
L1PA7	6897	501	8.30%	0.0112
L1PA6	3911	455	7.90%	0.0121
AluSx	289988	297	14.10%	0.0133
L1PA8	5805	365	10.30%	0.0139
L1PA10	4194	374	12.50%	0.0158
L1PA11	2723	370	14.20%	0.0181
L1PA13	6296	397	13.90%	0.0188
L1PB1	8237	456	13.50%	0.0191
L1PA14	2630	391	14.70%	0.0202
L1PA12	1156	361	15.10%	0.0202
AluJb	88254	294	20.10%	0.0209
L1PB2	2496	391	16.00%	0.0215
L1MA1	2697	442	14.50%	0.0215
L1PA15	5089	426	17.20%	0.0225
L1MA2	4076	491	15.30%	0.0226
AluJo	98469	292	21.90%	0.0234
L1MA3	5481	478	16.70%	0.0247
L1PA16	8862	458	18.00%	0.0252
L1PB3	2683	400	18.20%	0.0254
L1MA5	3337	402	20.70%	0.0305
L1MC1	8687	474	21.10%	0.0308
L1MA8	8187	390	21.70%	0.0312
L1MB3	11983	396	22.50%	0.0317
L1MA4	6702	430	20.70%	0.0321
L1MA6	3896	411	22.30%	0.0331
L1MA7	6447	369	23.10%	0.034
L1MA9	11244	378	24.60%	0.0351
L1MB8	11690	373	26.20%	0.0379
L1MC3	10570	534	29.40%	0.0439
L1ME1	18274	415	31.60%	0.0538
L1ME2	11886	367	32.50%	0.0547
MIR	258612	173	36.00%	0.0595
L2	25406	824	42.00%	0.0661
L3	27949	216	40.90%	0.0699

Table 1. Listed above are the 42 repetitive elements analyzed, including the number of copies found in the autosome, their average length, and the average percent of divergence from the consensus sequence. Note that only those exceeding a certain length threshold were kept. The last column lists the average value of the corrected transversion frequency.

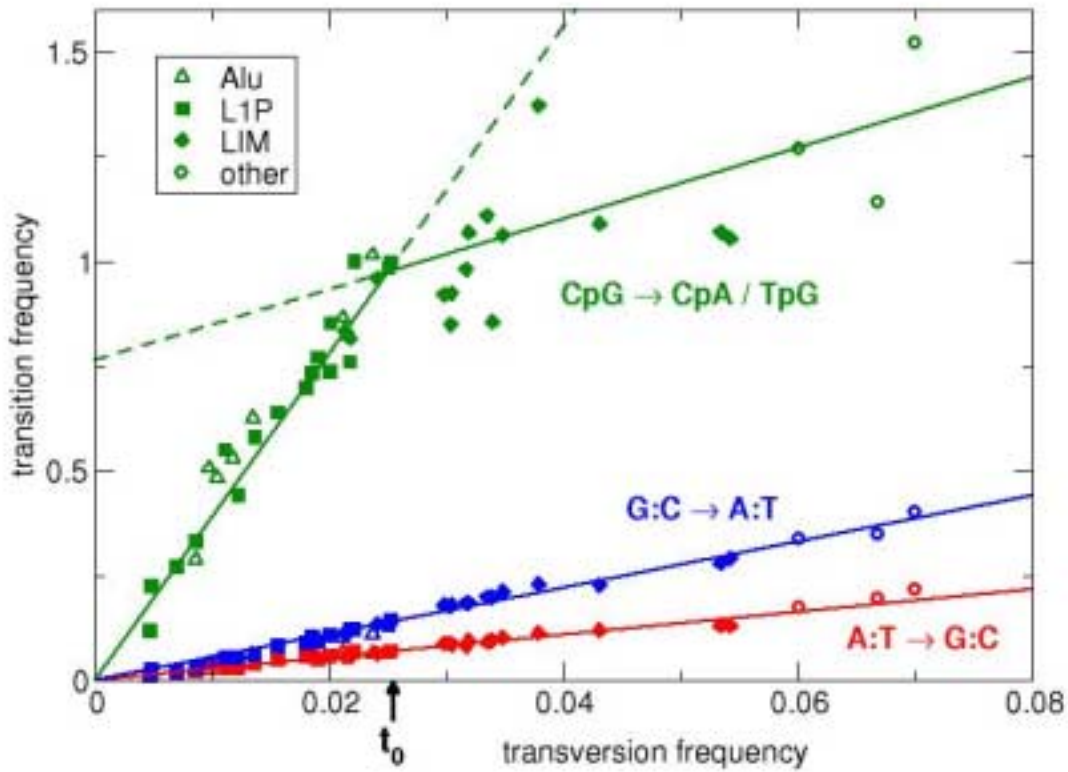


Figure 1. Genome-wide averages of the substitution frequencies for the 42 subfamilies of REs in human are determined using the ML-analysis. Plotted are the substitution frequencies for the two single-nucleotide transitions (blue and red) and the CpG-based transition (green) vs. the average transversion frequency. Each symbol represents the frequencies determined from one subfamily. (Statistical error is of the size of the symbol and not shown.) Different symbols distinguish the different families. The two single-nucleotide transition processes can be well fitted by a single line ($R=0.99$), while the CpG-based transition must instead be fitted by at least two lines joining at a time $t_0=0.025$.

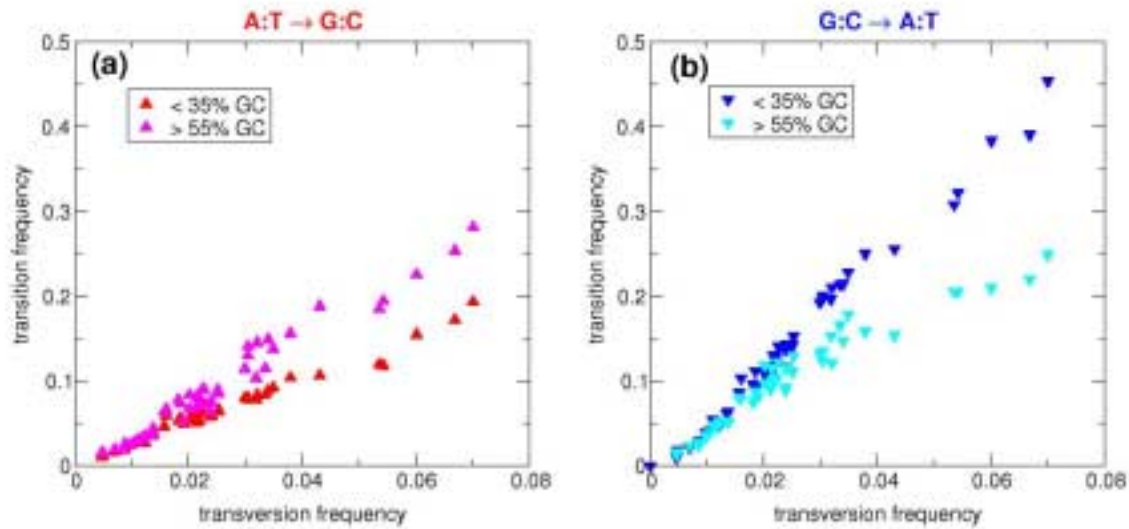


Figure 2. The two transition frequencies, A:T → G:C (a) and G:C → A:T (b), as determined by ML from REs found in regions with GC-contents above 55% and below 35%. The transition frequencies show little dependence on the regional GC-content for young REs with transversion frequencies below 0.02. However for the older REs (e.g., with transversion frequencies above 0.03), the differences in the transition frequencies in GC-poor and GC-rich regions are noticeable. Curiously the GC-dependence of the transition frequencies for the older REs are opposite for the two transition processes.

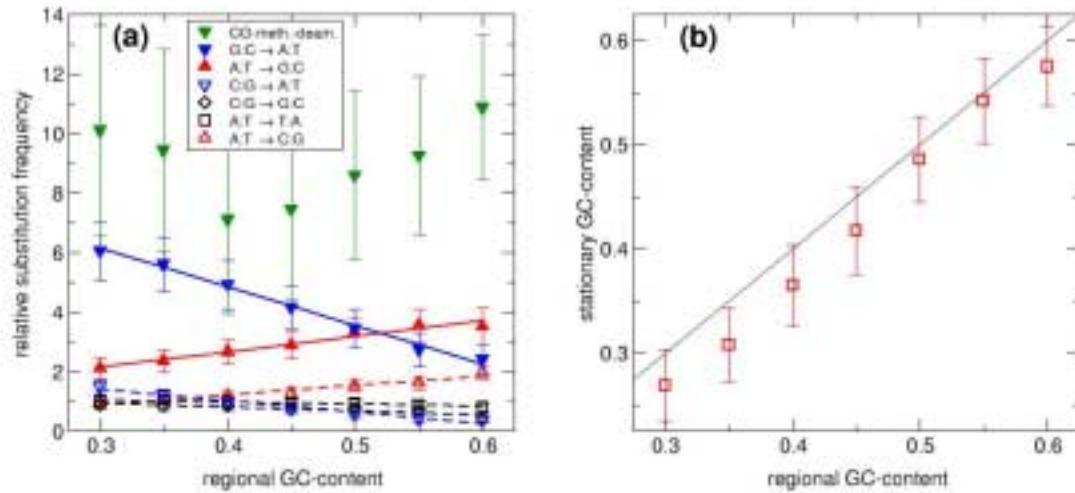


Figure 3. Substitution pattern prior to the “time” t_0 : (a) substitution frequencies (relative to the average transversion frequencies) as determined from REs with different regional GC-content. These frequencies were determined by straight line fits to data such as those shown in Fig. 2, for the portion with average transversion frequencies >0.03 . Colored lines are drawn to guide the eyes: we see that GC-enriching substitutions (red) increase and AT-enriching substitutions (blue) decrease with GC-content. (b) The expected *stationary* GC-content computed for the substitution rates shown in (a) for the different regional GC-contents. The straight black line indicates the equality of the stationary and regional GC-content.

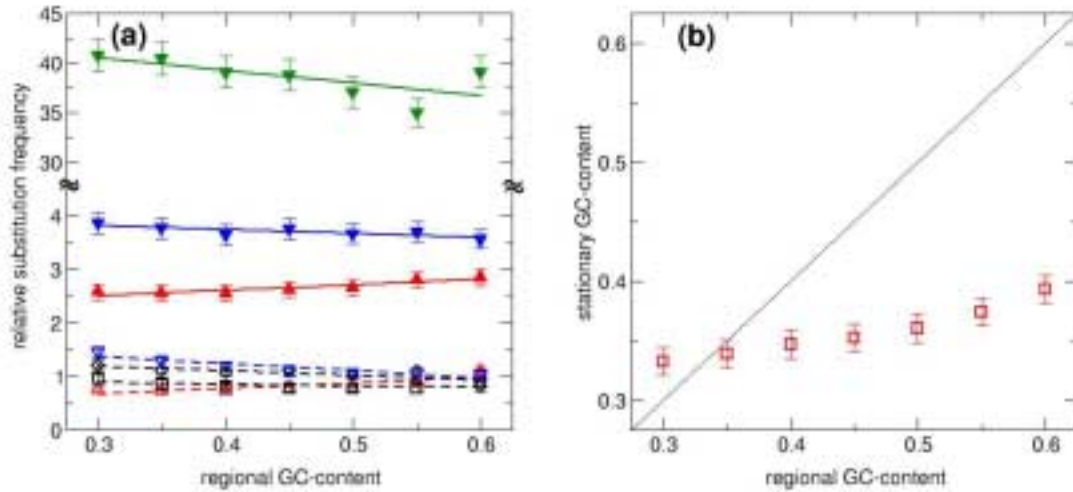


Figure 4. Substitution pattern after t_0 : (a) relative substitution frequencies determined and presented in the same way as in Fig. 3(a), but using only REs with average transversion rates <0.02 . Note the change in scale for the much larger CpG-based transition (in green). (b) The expected *stationary* GC-content computed using the GC-dependent substitution rates shown in (a). Note that it is far from the straight black line (the equality of the stationary and regional GC-content), indicating that the regional GC content is far from being equilibrated by the current rates. The eventual stationary GC-content according to the plot is 35-40%.

References

1. Filipowski, J., Thiery, J. P. & Bernardi, G. (1973) *J Mol Biol* **80**, 177-97.
2. Bernardi, G. (2000) *Gene* **241**, 3-17.
3. Eyre-Walker, A. & Hurst, L. D. (2001) *Nat Rev Genet* **2**, 549-55.
4. Coulondre, C., Miller, J. H., Farabaugh, P. J. & Gilbert, W. (1978) *Nature* **274**, 775-80.
5. Arndt, P. F., Burge, C. B. & Hwa, T. (2002) in *Proceedings of the 6th Annual International Conference on Computational Biology (RECOMB)*, G. Meyers *et al.* eds, pp. 32-38.
6. Hasegawa, M., Kishino, H. & Yano, T. (1985) *J Mol Evol* **22**, 160-74.
7. Kimura, M. (1981) *Proc Natl Acad Sci U S A* **78**, 454-8.
8. Kapitonov, V. & Jurka, J. (1996) *J Mol Evol* **42**, 59-65.
9. Britten, R. J. (1994) *Proc Natl Acad Sci U S A* **91**, 6148-50.
10. Britten, R. J., Baron, W. F., Stout, D. B. & Davidson, E. H. (1988) *Proc Natl Acad Sci U S A* **85**, 4770-4.
11. Jurka, J. & Smith, T. (1988) *Proc Natl Acad Sci U S A* **85**, 4775-8.
12. Mighell, A. J., Markham, A. F. & Robinson, P. A. (1997) *FEBS Lett* **417**, 1-5.
13. Jurka, J. (2000) *Trends Genet* **16**, 418-20.
14. Jurka, J. & Milosavljevic, A. (1991) *J Mol Evol* **32**, 105-21.
15. Smit, A. F., Toth, G., Riggs, A. D. & Jurka, J. (1995) *J Mol Biol* **246**, 401-417.
16. Smit, A. F. & Riggs, A. D. (1995) *Nucleic Acids Res* **23**, 98-102.
17. Gu, Z., Wang, H., Nekrutenko, A. & Li, W. H. (2000) *Gene* **259**, 81-8.
18. Press, W. H., Teukolsky, S. A., W.T., V. & B.P., F. (1992) *Numerical Recipes in C, The art of scientific computing* (Cambridge University Press, Cambridge).
19. Kumar, S. & Hedges, S. B. (1998) *Nature* **392**, 917-20.
20. Hedges, S. B., Parker, P. H., Sibley, C. G. & Kumar, S. (1996) *Nature* **381**, 226-9.
21. Easteal, S. (1999) *Bioessays* **21**, 1052-8; discussion 1059.
22. Eizirik, E., Murphy, W. J. & O'Brien, S. J. (2001) *J Hered* **92**, 212-9.
23. Murphy, W. J., Eizirik, E., Johnson, W. E., Zhang, Y. P., Ryder, O. A. & O'Brien, S. J. (2001) *Nature* **409**, 614-8.
24. Yi, S., Ellsworth, D. L. & Li, W. H. (2002) *Mol Biol Evol* **19**, 2191-2198.

25. Lander, E. S., Linton, L. M., Birren, B., Nusbaum, C., Zody, M. C., Baldwin, J., Devon, K., Dewar, K., Doyle, M., FitzHugh, W., Funke, R., Gage, D., Harris, K., Heaford, A., Howland, J., Kann, L., Lehoczy, J., LeVine, R., McEwan, P., McKernan, K., Meldrim, J., Mesirov, J. P., Miranda, C., Morris, W., Naylor, J., Raymond, C., Rosetti, M., Santos, R., Sheridan, A., Sougnez, C., Stange-Thomann, N., Stojanovic, N., Subramanian, A., Wyman, D., Rogers, J., Sulston, J., Ainscough, R., Beck, S., Bentley, D., Burton, J., Clee, C., Carter, N., Coulson, A., Deadman, R., Deloukas, P., Dunham, A., Dunham, I., Durbin, R., French, L., Grafham, D., Gregory, S., Hubbard, T., Humphray, S., Hunt, A., Jones, M., Lloyd, C., McMurray, A., Matthews, L., Mercer, S., Milne, S., Mullikin, J. C., Mungall, A., Plumb, R., Ross, M., Shownkeen, R., Sims, S., Waterston, R. H., Wilson, R. K., Hillier, L. W., McPherson, J. D., Marra, M. A., Mardis, E. R., Fulton, L. A., Chinwalla, A. T., Pepin, K. H., Gish, W. R., Chissoe, S. L., Wendl, M. C., Delehaunty, K. D., Miner, T. L., Delehaunty, A., Kramer, J. B., Cook, L. L., Fulton, R. S., Johnson, D. L., Minx, P. J., Clifton, S. W., Hawkins, T., Branscomb, E., Predki, P., Richardson, P., Wenning, S., Slezak, T., Doggett, N., Cheng, J. F., Olsen, A., Lucas, S., Elkin, C., Uberbacher, E., Frazier, M., et al. (2001) *Nature* **409**, 860-921.
26. Duret, L., Semon, M., Piganeau, G., Mouchiroud, D. & Galtier, N. (2002) *Genetics* **162**, 1837-1847.
27. Galtier, N. & Mouchiroud, D. (1998) *Genetics* **150**, 1577-84.
28. Bernardi, G. (1990) *J Mol Evol* **31**, 282-93.
29. Bernardi, G., Hughes, S. & Mouchiroud, D. (1997) *J Mol Evol* **44**, S44-51.
30. Hughes, S., Zelus, D. & Mouchiroud, D. (1999) *Mol Biol Evol* **16**, 1521-7.
31. Wolfe, K. H., Sharp, P. M. & Li, W. H. (1989) *Nature* **337**, 283-5.
32. Mouchiroud, D., Gautier, C. & Bernardi, G. (1988) *J Mol Evol* **27**, 311-20.
33. Burt, D. W., Bruley, C., Dunn, I. C., Jones, C. T., Ramage, A., Law, A. S., Morrice, D. R., Paton, I. R., Smith, J., Windsor, D., Sazanov, A., Fries, R. & Waddington, D. (1999) *Nature* **402**, 411-3.
34. Li, W. H. (1997) *Molecular Evolution* (Sinauer Associates, Sunderland, MA).
35. Yoder, J. A., Walsh, C. P. & Bestor, T. H. (1997) *Trends Genet* **13**, 335-40.

Supporting Information

Performance Evaluation

Generation of synthetically aged sequences. To test the performance of the ML method, we synthetically aged sequences starting from an ancestral sequence, using the following stochastic evolution procedure: Pick a base at random and allow one of the seven substitution processes we consider to occur with probability that is $1/1000$ of the corresponding substitution frequency ω ; repeat until every base was visited 1000 times on average. Scaling all ω 's by a single factor while keeping their ratios fixed, we can generate sequences evolved for various amounts of times with different degrees of divergence from the ancestor. The ratios themselves are the relative substitution frequencies and are independent of the amount of time the sequences have been aged for.

Estimation of the time-independent rates. To test the accuracy and limitation of our ML method in estimating the substitution frequencies, we synthetically evolved 200,000 copies of the ancestral MIR sequence (50 Mbp in total, comparable to the amount of MIR sequences found in the human genome) for various amounts of times, using substitution frequencies that are similar to those found from our analysis. We perform the ML analysis on the evolved sequence, and present the results of the analysis in Fig S1. The results (solid symbols) show fixed ratios between the transition and transversion frequencies, with slopes reflecting very accurately (within 1% relative errors) the substitution rates used in aging (given in the caption and shown as the straight lines in Fig S1). In the same figure, we present estimates of the same frequencies using the direct counting method (the open symbols). The latter gives poor estimates for the CpG-based transition frequencies due to the decay of most CpG's into either CpA or TpG for

sequences with transversion frequency above 0.01. The rate saturates to 0.5 for transversion frequency above 0.04.

Estimation of time dependent rates. In our ML analysis, we assumed that the relative substitution rates are time independent. Here we demonstrate that even if the substitution rates are time dependent, the ML analysis can still be used to give fairly accurate results, primarily due to the very large amount of sequence information in our dataset. Again we start with the 200,000 copies of the MIR ancestor sequences, and age them for various lengths of time t , using two different sets of substitution rates (past/present) that change at time t_0 . For $t < t_0$, we evolve the ancestor sequences using the present substitution rates throughout the time period t . For $t > t_0$, we first evolve the ancestral sequences using the past substitution rates for a time period $t-t_0$ and subsequently evolve using the present substitution rates for the remaining time t_0 . Next we apply our ML method to analyze sequences aged for each time period t , and plot the estimated transition and transversion frequencies for each t in Fig S2.

The relative single-nucleotide transition rates used are the same as those used to generate Fig S1; in addition, a 5-fold change in the CpG-based transition rate (from 8 to 40) is applied at $t_0=0.025$, mimicking what was observed (see the main text). From Fig S2, it is clear, that the CpG-based transition rate estimated by the ML method exhibits a sharp change at $t_0=0.025$. Moreover, the slopes of the computed frequencies provide good estimates of the actual time-dependent substitution rates (slopes of the straight lines) used in the aging process, with a relative error of $< 1\%$ through $t=0.05$, and 10% even at the longest time studied ($t=0.07$). Generally, the time where ML-estimate begins to deviate noticeably from the straight line is dependent on the total amount of sequence data. Note that the slope of the ML-estimate actually *overestimates* the rate. Thus, the magnitude of shift in the CpG-based transition rate deduced from Fig 1 can be even *larger* than what the change in slope naively suggests.

A similar test was performed to check whether a smaller change in the single-nucleotide transition rates could be captured using the same type of ML analysis. In Fig S3 we present the results of this test subjecting 20,000 copies of the ancestral MIR sequences to conditions similar to those observed in Fig 2. Here we find that the ML analysis gives excellent estimates for the relative substitution rates, which are indistinguishable from the applied rates before and after the time t_0 .

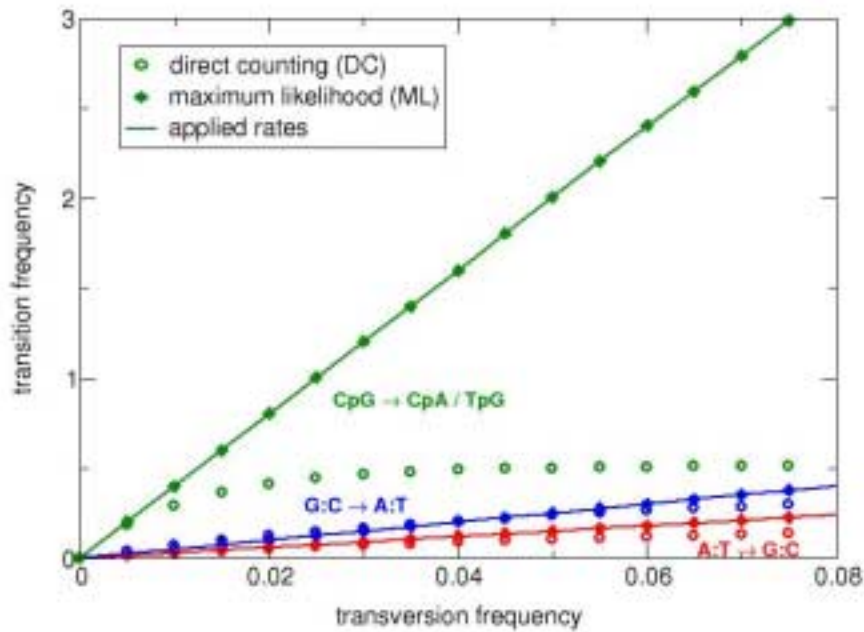


Figure S1 Comparison of the maximum likelihood (ML) and the direct counting (DC) method: 200,000 copies of MIR sequence (50Mbp in length) were synthetically evolved according to a stochastic model with equal transversion rates and differing transition rates ($A:T \rightarrow G:C$ rate=3x, $G:C \rightarrow A:T$ rate=5x, and CpG-based transition rate=40x that of the transversion rate respectively, as indicated by the slopes of the straight lines), for various periods of time. Plotted are the estimated substitution frequencies for the two single-nucleotide transition processes (blue and red) and the CpG-based transition (green) versus the average transversion frequency, as determined by the ML (solid symbols) and DC (open symbols) methods. The ML method is able to recover the “true” substitution frequencies (the solid lines) throughout the studied regime, while the DC method quickly saturates.

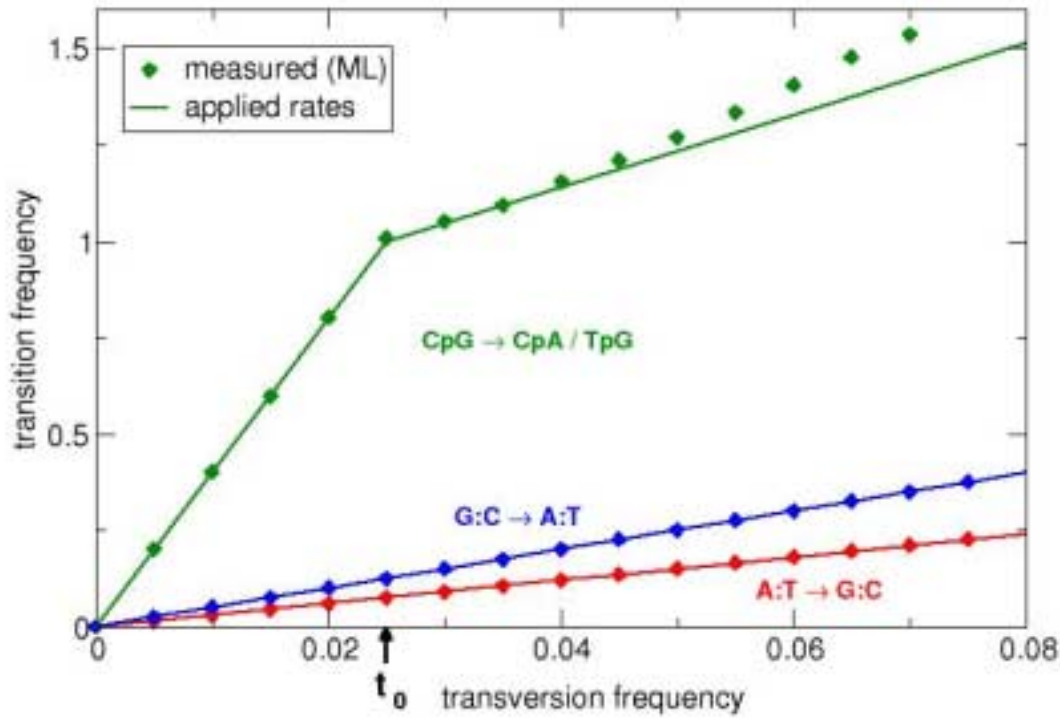


Figure S2 Performance test with time-dependent substitution rates: 200,000 copies of MIR consensus sequence (50Mbp in length) were synthetically evolved according to a stochastic model which includes a change of the CpG-based transition rate at $t_0=0.025$, similar to what is observed in Fig 1. The relative A:T→ G:C rate is 3 and G:C→ A:T rate is 5 as in Figure S1. The relative CpG-based transition rate is 40 for $t < t_0$ and 8 for $t > t_0$. The data points represent the estimated substitution frequencies determined by the ML method. Note that the slope of the data points provide a reasonable estimate of the true rates (the solid lines) for most of the time period studied.

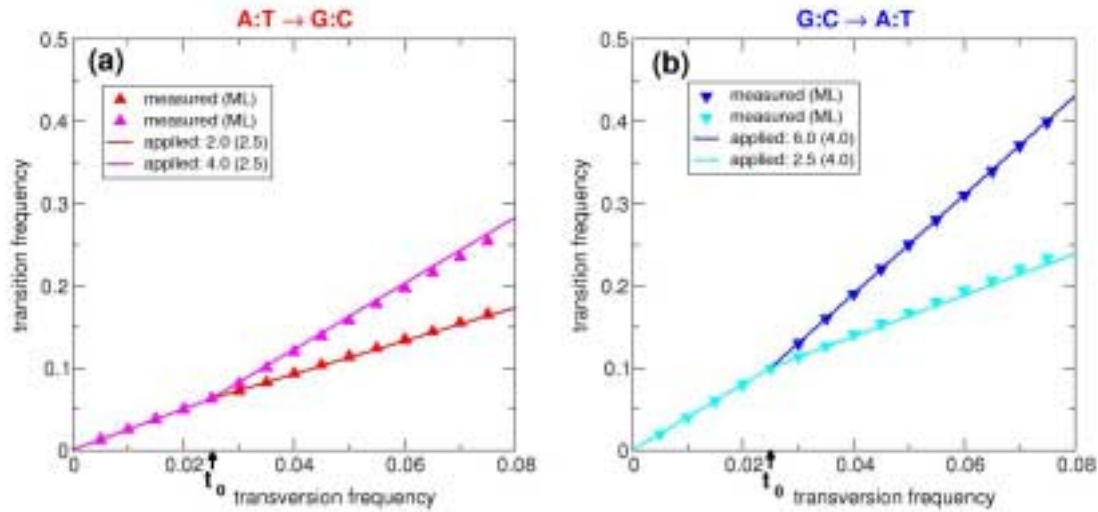


Figure S3 Same test as in Figure S2, but with fewer (20,000) copies of the ancestral MIR sequence (6Mbp in length) and smaller changes in the single-base transition rates at $t_0=0.025$, mimicking the situation of Fig 2. The graphs show the measured substitution frequencies for the A:T→ G:C transition (a) and the G:C→ A:T transition (b). Each graph present data for two tests using substitution frequencies as observed in GC-poor and GC-rich regions. The transversion rates remained constant in all sets. The values for the relative transition frequencies before (and after) t_0 are as labeled and represented by straight lines.